Final report

First principles calculations for surfaces; surface stress and segregation
OTKA T 48827

The aim of the project during the last five years was to carry out quantum-mechanical calculations for describing the surface and bulk properties of metals, alloys and compounds. We believe that as a result of this project we have managed to get a deeper insight in the surface physics for a wide range of materials and different surface phenomena. In these descriptions we have applied the density functional theory, and partly the electronic structure calculation methods that we have developed earlier.

In 2008 we have organized a Workshop on "New challenges in the Electronic Structure of Complex Materials" (June 29 - July 1, 2008). The purpose of the meeting was to provide an overview on our recent activity about studying the bulk and surface electronic properties of metals and alloys, and stimulate cooperation in these fields. The number of participants was 40 from ten different countries.. The workshop was sponsored by the Research Institute for Solid State Physics and Optics, and two OTKA projects (T046773, T048827).

During the project we have published several papers (48 publications, total impact factor 136.16) in a large variety of fields of computational material science. Among these results in this report we will focus on three main areas: *i/* Surface relaxation and stress of transition metals, *ii/* Surface segregation of random alloys, and *iii/* Reconstruction of semiconductor surfaces.

i/ Surface relaxation and stress of transition metals

The determination of the surface geometry of solid surfaces is one of the basic questions of surface science. Transition metal surfaces are of particular interest, since they act as catalysts in various reduction and hydrogenation reactions. It is well known that real surfaces of pure metals can adopt different structures from those of ideally truncated crystals. During relaxation only rigid inward or outward displacement of the atomic layers occurs, while in the case of reconstruction the displacement of atoms may alter the two-dimensional symmetry of the surface. Experimental studies have demonstrated that the surface layer of clean transition metal surfaces relaxes inward, i.e. the interlayer distance between the topmost two atomic layers is smaller than that of the bulk. Outward expansion of the top layer has also been found for some surfaces of noble metals. The top layer relaxation is often accompanied by relaxation of the subsurface atomic layers, resulting in an oscillatory multilayer relaxation.

Anomalous surface relaxation of hcp metals

In this work, using density-functional calculations, we show that the layer relaxation for the close-packed surfaces of 5d transition metals follows a trend similar to that of the 4d metals. Using these theoretical results, we carry out a systematic analysis of the surface relaxation in nonmagnetic transition metals and reveal the electronic origin of the observed anomalous relaxation for the (0001) surface of the hexagonal-close-packed (hcp) Zr, Tc, Hf, and Re. We demonstrate that these anomalies can be explained by the particular shape of the Fermi surface for these metals, which are also reflected by the flat and degenerate d bands close to the Fermi level in the L-A-H plane of the hcp Brillouin zones. We mention that the same peculiar behavior of the electronic band structure is responsible for the observed unusually soft [001] longitudinal optical (LO) phonons in the above hcp metals. We call attention to the fact that these phenomena are related to the particular response of the bulk electronic system to external perturbations, regardless whether these perturbations are displacements of atoms in a lattice or creation of a surface. This response is determined mainly by the bulk electronic structure, and the characteristic behavior of the screening charge density can be traced back to the topology of the Fermi surface (similar to the "nesting condition" in the theory of charge-density waves). For hcp metals, especially for Tc and Re, for the screening of perturbations along the [0001] direction, the special shape of the Fermi surface results in a screening charge which can explain the observed anomalous behavior for both kinds of phenomena.

In Fig. 1, we compare the present values for d_{12}-s obtained for the 5d metals with those reported in the case of 4d metals (inset, d_{12} stands for the surface change of the distance between the first and second layer, relative to the bulk). It has been shown that the top-layer surface relaxation for nonmagnetic transition metals follows a generic trend across the series with decreasing relaxation as we approach the noble metals. In general, both the 4d and 5d series follow this trend. For Pd, Pt, and Au, the surface relaxation changes sign, and the surface atoms exhibit a slight outward displacement. Beyond this generic trend, however, for some hcp metals an anomalous behavior can be observed. In particular, groups IVA (Zr and Hf) and VIIA (Tc and Re) show significantly larger relaxation than groups IIIA (Y and La) and VIA (Ru and Os), respectively. In the following, we will investigate the electronic origin of the obtained anomalous surface relaxations for Zr, Hf, Tc, and Re. Furthermore, we will point out that the slow decay of the relaxation for Tc and Re is connected to the unusually soft optical phonons in these metals. One possible way to approach the problem of surface relaxations is by looking at the surface as a two-dimensional defect with a potential which is screened toward the bulk metal. It is well known that free surfaces cause Friedel oscillations in the charge density toward the bulk metal. The periodicity of the Friedel oscillation is twice the Fermi wave vector k_F , and it is generally incommensurate with the relevant lattice constant of the metal. This causes the layer relaxation to fall off quickly toward the bulk. However, if the lattice constant and $2k_F$ are commensurate, then the layer relaxation and the Friedel oscillation strengthen each other, which results in a slowly decaying layer relaxation toward the bulk. We can find the periodicity of the Friedel oscillation for the (0001) surface of groups IVA and VIIA hcp metals by investigating their Fermi surfaces.

The Fermi surfaces from Fig. 2 were obtained from density functional calculations and correspond to the zone-edge bands of Zr, Tc, Hf, and Re, respectively. In all cases, small hole pockets appear at the zone edge. In the cases of Zr and Hf, the hole pockets are located at the H point (the corner of the hexagonal Brillouin zone), while in the cases of Tc and Re they are located at the L point (the half point of the line connecting the neighboring corners of the hexagon). The presence of these hole pockets allows for low-energy excitations in the k_z direction, as marked by the arrows in Fig. 2. As the hole pockets are at the edge of the zone, the wave vectors connecting them correspond to the periodicity of the lattice along the z axis, i.e., to the c lattice constant of the hexagonal lattice. This is especially prominent for Tc and Re as their hole pockets are located extremely close to the zone boundary. In the case of the other 4d and 5d transition metals, there are no similar hole pockets in the Fermi surface and therefore, the wave vector of the low-energy excitations responsible for the Friedel oscillations is always incommensurate with the lattice periodicity perpendicular to the surface.

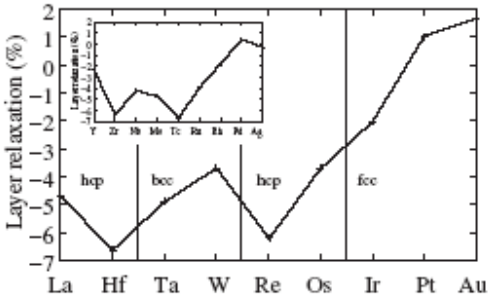

Figure 1Top-layer relaxations for the close-packed surfaces of 5d transition metals. The inset shows results obtained for the 4d transition metals. In both series, an anomalous behavior is found for groups IVA (Zr and Hf) and VIIA (Tc and Re) metals.

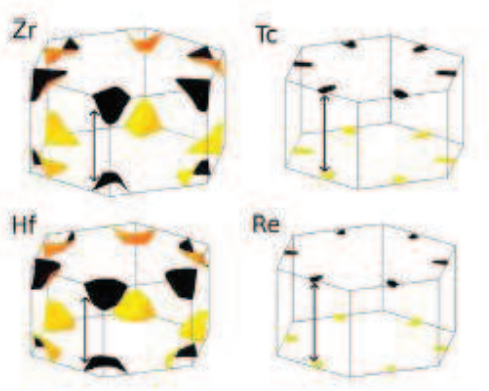

Figure 2 Fermi surface pieces obtained from the zone-edge bands of Zr, Tc, Hf, and Re, which are not present in Ru and Os. In the case of Tc and Re, where a nesting condition is nearly satisfied, the wavelength of oscillations is close to the c lattice constant.

Surface stress for the 4d and 5d metals

In contrast to the surface energy, the surface stress is drastically influenced by layer relaxation. According to a simple model described by Ibach, upon cleaving a metal surface the electronic charge density of the broken bonds is redistributed between surface atoms and their backbonds. This leads to increased charge density between surface atoms. However, lattice constraint by subsurface layers hinders inplane relaxation of surface atoms, resulting in the tensile (positive) surface stress on metal surfaces. The first-principles calculations performed so far confirm that the surface stress on clean metal surfaces is tensile. Furthermore, strengthening of the backbonds of surface atoms results in inward relaxation of the top layer. Nichols et al explained the surface stress change during surface relaxation in terms of a jellium model and performed ab initio DFT calculations to describe the outward relaxation of the Au(111) surface. They have suggested that the shift of the energy bands to lower energies, i.e. the depleted surface density of states near the Fermi level, is the driving force for the expansion on the Au(111) surface.

In Figures 3 and 4 we show our surface energy and stress values for the most closely packed surfaces of the 4d and 5d series. Comparing the figures we can see that both the surface energy and surface stress values reflect the parabolic trend observed for the cohesive energy of the transition series, i.e. the values are smaller at the beginning and at the end of the series and larger in the middle. In the second half of the 5d series the surface stress values are much larger than those of the surface energy, which has significant consequences on the reconstruction of these surfaces.

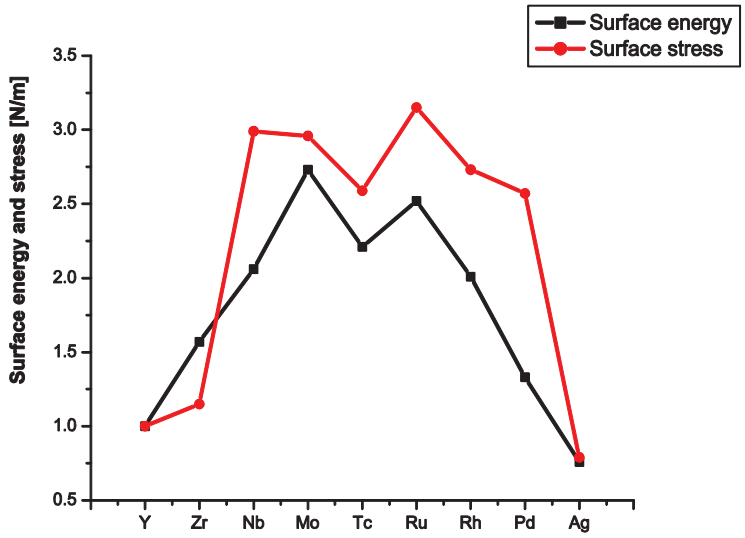

Figure 3 Calculated surface energy and stress for the 4d series.

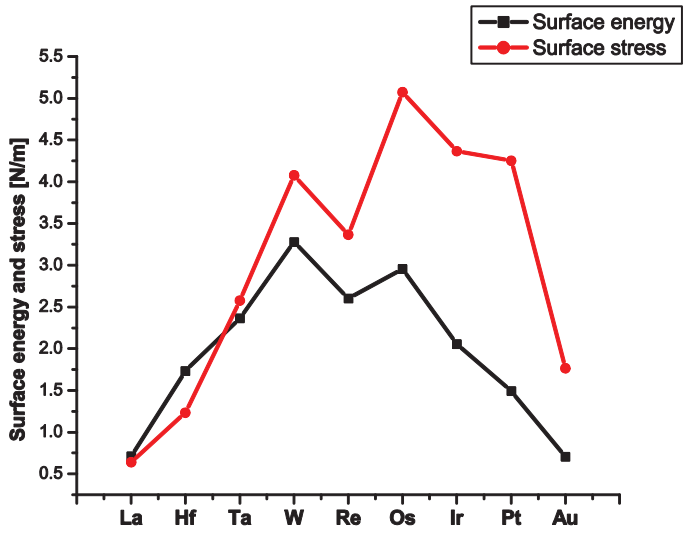

Figure 4 Calculated surface energy and stress for the 5d series.

Table 1 Estimated elastic energy change for the most closely packed surfaces (mcp) of Re–Au. The excess surface stress values (τ−γ)mcp are also shown.

	$(\tau-\gamma)_{mcp}$ (J m^{-2})	$(\tau-\gamma)_{100}$ (J m^{-2})	G (GPa)	b (Å)	$Gb/10$ (J m^{-2})
Re	0.73	—	180	2.773	5.0
Os	2.12	—	223	2.754	6.1
Ir	2.31	0.41	209	2.741	5.7
Pt	2.76	1.47	61	2.812	1.7
Au	1.06	1.21	26	2.951	0.8

Intuitively it is straightforward to assume that a large surface stress can result in a surface reconstruction. This idea is described quantitatively in Cammarata's model (first proposed by Herring, and later extended by Cammarata). Several effects should be taken into account in order to predict if a surface will reconstruct or not. First of all it is obvious that there is a remarkable energy gain if a surface with tensile stress is compressed and the surface strain energy is reduced. This energy gain is proportional to the surface stress τ. At the same time, however, the density of atoms at the surface is increased, i.e. atoms should be transferred from the bulk to the surface, which is roughly proportional to the surface energy γ . Therefore the driving force for surface reconstruction is proportional to the excess surface stress $\tau - \gamma$. This energy gain should be compared to the energy contribution associated with the energetically unfavorable sites in the reconstructed layer. In Cammarata's model this energy contribution is described by the energy change due to the formation of a dislocation using the continuum elastic theory: αGb, where G stands for the shear modulus, b is the magnitude of the Burgers' vector of the reconstruction and $\alpha = 4\pi(1-\nu))-1 \cong 0.1$ (ν stands for Poisson's ratio). Reconstruction is expected if $\tau - \gamma$

> αGb. In Table 1 we have listed these elastic energy contributions for Re–Au. According to these, reconstruction is expected for Au(111), Au(100), Pt(111) and perhaps Pt(100). In all other cases the excess stress is not enough to compensate for the elastic energy loss. Experimentally, surface reconstructions are observed for Ir(100), Pt(100) , Au(100), Au(111) and Pt(111). For the Ir(100) we have no explanation for the reconstruction, although in this case we do not expect that the formation of a quasi-hexagonal, close packed top surface layer is properly described by Cammarata's model. For all other cases our predictions are in good agreement with the experimental observations.

ii/ Surface segregation of random alloys

We have worked out a method to calculate the surface concentration profile for random alloys. During this type of calculations we minimize the free energy of the system as a function of the concentrations in different surface layers. An interesting application of the theory is the Fe-Cr system with low bulk Cr concentration, the ferritic stainless steals.

In Fe-Cr alloys, a drastic decrease in the corrosion rate with chromium addition occurs within a narrow concentration interval (9–13% Cr), making the transition from the iron-type to the noncorrosive behavior quite abrupt. Alloys in the latter category form the basis of the so-called ferritic stainless steels. Phenomenological models have been introduced to describe the passivity of stainless steels, and today there is a generally accepted mechanism based on the formation of a protective Cr-rich oxide surface film. On the other hand, despite the numerous experimental and theoretical investigations on alloy surfaces, the observed threshold behavior in the Fe-Cr system has remained less well understood. There is experimental evidence for Cr-enriched alloy surfaces in the stainless regime at high temperatures. From the theoretical side, all studies have focused on dilute alloys and most of them predicted the stability of Cr-free surfaces. However, it seems very unlikely that these pure Fe-terminated surfaces would facilitate the development of the passive oxide film and provide the self-healing property in the noncorrosive regime. In the present work, we aim to resolve the above contradiction. We investigate the behavior of Fe-Cr surfaces as a function of bulk composition within an extended concentration range and try to reveal the mechanism that can stabilize Cr-containing surfaces in high-Cr alloys. Our ability to address this problem at a first-principles quantum-mechanical level has become possible through the exact muffin-tin orbital (EMTO) method based on density functional theory in combination with the generalized gradient approximation. This approach has proved to be an accurate tool in the theoretical description of Fe-based random alloys. At ambient conditions, elemental Fe orders ferromagnetically while Cr has an incommensurable antiferromagnetic state, which can be approximated by a commensurable (B2 structure) antiferromagnetic state. The Fe-Cr alloys, except the high-temperature Fe-rich *gamma-phase* and the *sigma-phase* observed around equimolar concentrations, adopt the body centered cubic (bcc) structure of *alpha*-Fe. Here we focus on the technologically important $Fe_{1-c}Cr_c$ alloys with $c<0.25$. At normal operating temperatures, these bcc alloys are ferromagnetic with Curie temperatures around 900–1050 K. For $c<0.1$ and $T>600$ K, the Fe-Cr system is fully

miscible, whereas nucleation or spinodal decomposition driven clustering occurs at higher Cr concentrations. Nevertheless, it has been shown that the energetics of Fe_{1-c} Cr_c alloys with $c<0.2$ are well described using the substitutionally disordered ferromagnetic bcc phase.

In the present magnetic systems, surface magnetism reduces the surface energy of open surfaces to the extent that the usual anisotropy of the surface energy is reversed. In particular, the magnetic contribution to the surface energy of the (100) facet of pure Cr (Fe) is about −50% (−41%) compared to −2% (−16%) obtained for the close-packed (110) facet. Accordingly, the most stable surfaces for pure Cr and for Fe-rich Fe-Cr alloys are the (100) crystal facet of the B2 lattice and the (100) crystal facet of the bcc lattice, respectively. We modeled the Fe-Cr system by considering two distinct subsystems: one with surfaces (the so-called surface subsystem) and one without surfaces (the bulk subsystem). The two subsystems were allowed to exchange atoms with each other. The bulk subsystem acted as a reservoir for the surface, enabling a change in the surface composition without finite change in the bulk composition. The surface subsystem for Fe-Cr alloys was described by periodically repeated atomic slabs formed of eight (100) atomic layers and separated by vacuum layers of thickness equivalent to four atomic layers. Similar slab geometry was adopted for modeling the pure Fe and Cr surfaces. In the case of alloys, the concentration in the top monolayer was allowed to relax and all the other layers had the bulk composition.

The surface concentrations were obtained by minimizing for each temperature T the grand canonical potential of the surface subsystem. At T=0 K, this leads to the condition that the difference between the effective chemical potentials should be equal to the equilibrium segregation energy. The latter vanishes for an equilibrium concentration profile, where all the alloy components have finite concentrations. The effective chemical potentials were calculated as the energy change when a Cr atom was exchanged with Fe. For finite temperatures, the entropy was approximated by the configurational entropy. We note that in Fe-rich alloys and for temperatures well below the magnetic transition temperature, the vibrational and magnetic entropy terms are expected to have negligible effect on the equilibrium concentration profile.

In Fig. 5, we observe a sharp change in the surface Cr content for alloys encompassing 8–12% Cr. Accordingly, at low temperatures there is practically no Cr present at the surface for $c<0.08$. This means that thermodynamically the most stable surfaces are the Fe-t terminated surfaces. For alloys with bulk Cr concentration above 8–9%, the Cr containing surfaces start to become stable. The actual amount of Cr at the surface for $c \cong 0.1–0.2$ is close to, or slightly higher than, the Cr concentration in the corresponding bulk alloy, reaching a maximum of 20–27% (depending on temperature) for $c \cong 0.12–0.15$. The predicted stability of Cr-enriched surfaces in the stainless region is fully supported by experiments. A quantitative comparison shows that the present theoretical surface Cr content is below the observed values of 45% for c=0.13 and 69% for c=0.25. However, it is important to note that these experiments were performed on samples heated to 973 K under ultrahigh vacuum. At this temperature, the Fe-Cr alloys are close to their magnetic transition, which is expected to have a substantial effect on the thermodynamics of bulk

and surface alloys. The demonstrated transition in the surface Cr concentration in Fe-Cr alloys (Fig. 5) clearly shows the characteristics of the experimentally observed compositional threshold.

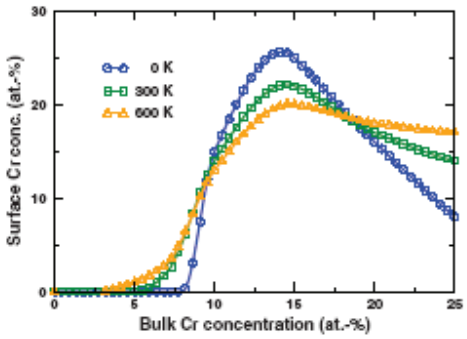

Figure 5 Theoretical surface concentration of chromium for ferromagnetic Fe1−cCrc alloys as a function of bulk Cr concentration (in at. %)

To interpret the results we call attention to the fact that bulk Fe-Cr alloys have a broad and slightly skewed miscibility gap, allowing the solubility of a small amount of Cr in Fe but not vice versa. In good agreement with other theoretical predictions, we find that at low Cr concentrations the ferromagnetic solid solutions have slightly negative mixing enthalpies and therefore they are stable at all temperatures. It has been demonstrated that the limited solubility of chromium in iron is connected to the complex magnetic interactions characteristic of solid solutions between antiferromagnetic (Cr) and ferromagnetic (Fe) species. These interactions originate from magnetic frustrations due to the strong antiparallel coupling between Cr and the Fe matrix and also between different Cr atoms.

Finally, we point out that the strongly nonlinear change of the surface Cr content versus bulk composition is due to the delicate balance between bulk and surface effects. In particular, the lack of Cr at the surface of Fe-rich alloys is a direct consequence of the anomalous mixing of Fe and Cr at low Cr concentrations, which in its turn has a magnetic origin. This finding has important implication in modern materials science as it offers additional rich perspectives in the optimization of high-performance steel grades.

iii/ Reconstruction of semiconductor surfaces

In order to understand the physics behind several phenomena taking place on semiconductor substrates, such as chemical reactions, epitaxial growth, and self-assembly of nanostructures, it is necessary to know the detailed atomic structures of adsorbate-stabilized semiconductor surfaces. The common principles for these surfaces are as follows: (a) removal of the dangling bonds, (b) stress relief of the surface layer, and (c) tendency to a semiconducting rather than metallic band structure. A modification of the last principle is the well-known electron counting model (ECM) for compound semiconductors. Based on ECM, the surface energy is reduced when all dangling bonds of the electropositive atoms (e.g., group-III), which lie above the Fermi energy, become

empty of electrons and those of the electronegative atoms (e.g., group-V), which lie below it, become doubly occupied. For III-V(100) semiconductor surfaces, which several technologies such as wireless and optical communications are based on, the ECM principle predicts a semiconducting reconstruction with vacant dimer sites. This means that part of paired surface atoms is missing, and the (2 x 4) or (4 x 2) unit cells are the smallest ones on V- and IIIstabilized III-V(100) surfaces. Although, in general, the observed reconstructions agree well with ECM, there are indications for anomalous surfaces. The semiconducting P-stabilized (2 x 1) reconstruction on InP(100) is one of the most interesting examples. Such a small unit, however, should include a half-filled dangling bond, and thus the (2 x 1) surface without any dimer vacancies should be metallic and unstable. Nevertheless, later this P/InP-(2 x 1) has been shown to be stabilized by hydrogen adsorbate. Thus, the recent finding that a group-V adsorbate (Bi) induces well-ordered (2 x 1) reconstructions on various III-V(100) surfaces is challenging. In general, understanding the properties of these Bi/III-V-(2 x 1) surfaces is crucial to determine the detailed physical mechanisms of III-V reconstructions and the epitaxial growth of III-V materials for electronics, the latter being essentially a surface process proceeding via V-stabilized reconstructions. In particular, Bi has been utilized as surfactant in the growth and also alloyed with III-V's (e.g., $GaAs_{1-x}Bi_x$) to produce spintronics materials.To realize why the Bi surfactant on the growing surface changes the characteristics of device materials (e.g., leads to smoother interfaces and higher photoluminescence intensity), it is of great importance to understand the fundamental properties of the Bi/III-V surfaces.

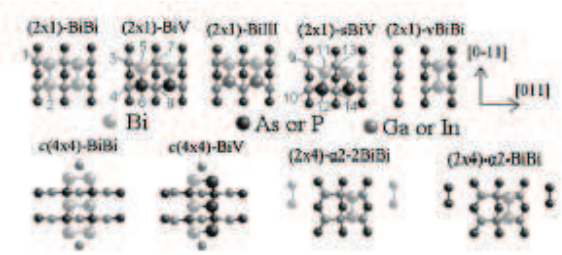

Figure 6 Atomic models for Bi-induced (2 x 1), (2 x 4), and C(4 x 4) reconstructions on GaAs and InP.

The theoretical calculations were performed using the ab initio DFT total-energy code with the local density approximation. The approach is based on planewave basis and projector augmented wave method (VASP). The (2 x 1) reconstructions (Fig. 6) were simulated with (2 x 2) slabs including 13 atomic layers and treating the Ga 3d electrons as valence electrons. The relative stabilities of (2 x 1), (2 x 4), and c(4 x 4) were calculated using (4 x 4) slabs with 9–10 atomic layers and keeping all d electrons in the core. Pseudohydrogenated slabs were used with the cut off of 280 eV. The number of k points in the Brillouin zone was 9 and 4 for (2 x 2) and (4 x 4) slabs, respectively. The surface energies were evaluated as a function of chemical potentials (γ) in the standard way.

The theoretical phase diagrams for Bi/GaAs and Bi/InP [Figs. 7(a) and 7(b)] demonstrate the stability of the (2 x 1) reconstructions. Calculations also indicate that the Bi-stabilized (2 x 4)-α 2 reconstructions appear when the Bi amount decreases. Indeed, the α 2 phases

are found in experiments only after heating the (2 x 1) surfaces to desorb Bi partly. According to Figs. 7(a) and 7(b), the (2 x 4)-$\beta 2$ structure, being stable on several III-V surfaces, is not stabilized by Bi. This finding agrees well with the present and former STM measurements, in which $\beta 2$ has not been observed. The Bi/III-V-c(4 x 4) structures, seen in the upper left corner of Figs. 7(a) and 7(b), were not found in our measurements. This may be attributed to the fact that in experiments, the III-rich substrates were used for Bi deposition. Theory shows that only one type of the (2 x 1) structure is stable [Figs. 7(a) and 7(b)]. This is composed of symmetric Bi-Bi dimers (labeled as BiBi in Fig. 6). On the other hand, the reconstructions formed can be affected by surface kinetics, which depend on the surface preparation, and are not taken into account in the above thermodynamic diagrams.

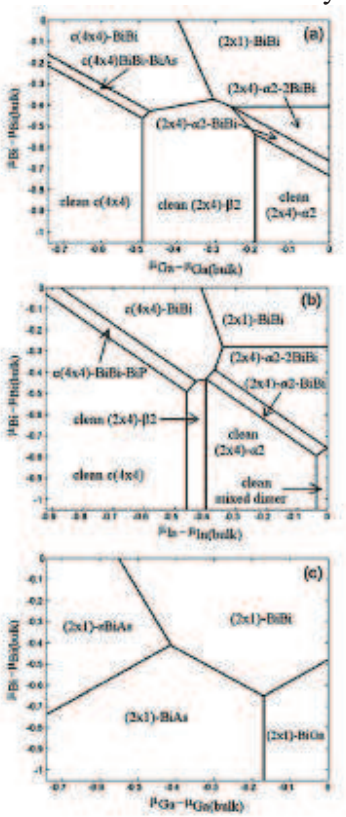

Figure 7 Phase diagrams for Bi/GaAs (a) and Bi/InP (b). Relative stabilities of (2 x 1) structures on Bi/GaAs (c).

Therefore, here we also consider other possible (2 x 1) phases. The diagram of the most favored phases is shown in Fig. 7(c). Schematic plots (with selected bond lengths) for these phases are given in Fig. 6. Surprisingly, calculations show that the mixed Bi-As and Bi-P dimers are buckled about 0.4–0.5 A°. This is in contrast with previous findings for group-V dimers, and it is supported below by the comparison of our measured and calculated STM images. Regarding the electric conductivity, our calculated electronic structures (not shown) indicate that BiBi, vBiBi, BiGa, BiAs, and BiP are metallic, as expected, and sBiAs and sBiP are semiconducting with the energy gap of about 0.5 eV. This is reasonable because the number of available electrons in sBiAs and sBiP is exactly

the same as needed to fill all the bonds. In the following, by comparing the calculated and measured core-level and STM results, we identify those phases that explain the observed Bi/III-V-(2 x 1) reconstruction.

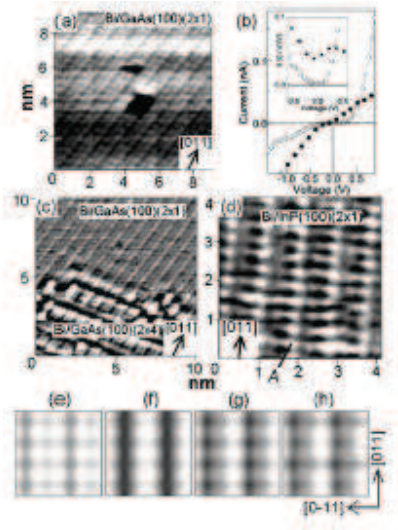

Figure 8 (a) Filled-state STM image of Bi/GaAs-(2 x 1); (b) I(V) curves (c) Filled-state STM image of Bi/GaAs, which consists of both (2 x 1) and (2 x 4) phases; (d) Filled-state STM image of Bi/InP-(2 x 1) (e)–(h) Calculated filled-state STM images.

The STM image of Bi/GaAs-(2 x 1) is shown in Fig. 8(a). Its comparison with the calculated images in Figs. 8(e)–8(h) demonstrates the existence of symmetric Bi-Bi dimers. Furthermore, valence-band photoemission (not shown) reveals a substantial emission at the Fermi energy, supporting the presence of metallic areas on Bi/GaAs-(2 x 1). [Our valence-band measurments reveal metallic areas also on Bi/InP-(2 x 1), agreeing with the STM results. Indeed, the I(V) curve and its differential [Fig. 8(b)], obtained for the same region as Fig. 8(a), show the metallic character of the Bi/GaAs-(2 x 1) area. These findings confirm that the BiBi areas appear on Bi/GaAs-(2 x 1), in good agreement with our total-energy results [Fig. 7(a)]. The STM image of the high-temperature surface [Fig. 8(c)], including both (2 x 1) and (2 x 4) phases, suggests the existence of another (2 x 1) phase(s), which agrees with the calculated BiAs [Fig. 8(g)] and sBiAs [Fig. 8(h)] images. We cannot distinguish between them because of the limited resolution in Fig. 8(c). However, the I(V) curve and its differential [Fig. 8(b)] from the high-temperature (2 x 1) phase indicate semiconducting sBiAs. Its presence is also supported by our photoemission findings.

A third structure is found on InP: the calculated BiP image (BiP is metallic), similar to the BiAs image in Fig. 8(g), describes the best our STM image for Bi/InP-(2 x 1) [Fig. 8(d)]. This allows us now to identify the white protrusion A from Fig. 8(d) as an upper Bi atom of the buckled Bi-P dimer. The previous results suggest also the appearance of semiconducting sBiP areas.

To answer the question of why the Bi/III-V-(2 x 1) structures are stable, we recall that their stability was intuitively proposed to be due to surface stress relief. The present results provide clear evidence for that. Although the stresses do not vary significantly between Bi/GaAs-(2x 1)-BiBi and various (2 x 4) and hypothetical (2 x 1)-AsAs and (2 x 1)-SbSb structures, the stress relief due to the relaxation of the adsorbate atom is found to be the largest on (2 x 1)-BiBi. For example, the dimerization decreases the surface stress by 105.3, 50.0, and 41.1 meV/A^2 on (2 x 1)-BiBi, -SbSb, and -AsAs, respectively. Upon dimerization, the change in the dimer bond length is found to be largest, and therefore, to a large extent, the above changes in the surface stress may be attributed to the stress relief experienced by the dimers. The largest relief on (2 x 1)-BiBi describes the fact that Bi atoms have the largest tendency to dimerize. This is because Bi atoms have a strong attractive interaction on the (1 x 1) atomic positions as a result of their large size. We conclude that the above mechanism is the main driving force behind Bi/GaAs-(2 x 1)-BiBi. Another stabilizing factor appears in the calculated density of states (DOS, not shown): DOS near the Fermi energy is lower on (2 x 1)-BiBi than on (2 x 1)- AsAs and -SbSb; i.e., a pseudogap forms on (2 x 1)-BiBi. [A certain number of states still appears at the Fermi energy on (2 x 1)-BiBi, agreeing with the metallic character found above.] The pseudogap may also be associated with the Bi size. The Bi-Ga backbond is long, resulting in larger pz occupation compared to px and py occupations in contrast to (2 x 1)-AsAs. Consequently, the sp3 hybridization changes to the p3 hybridization, which is also revealed in the angles between backbonds (90.39^0). Thus, this hybridization leads to the opening of the pseudogap at the Fermi energy.